Proceedings World Geothermal Congress 2020+1
Reykjavik, Iceland, April - October 2021

Thermodynamic Performance of Combined Heat and Power (CHP) System for EGS with Different Cycle Configurations

Tailu Li[1], Nan Meng[1], Yanan Jia[1], Yanhua Yao[2], Yingchao Zhu[2]

1 School of Energy and Environmental Engineering, Hebei University of Technology, Tianjin 300401, China

2 Water Supply Company of Liaohe Oilfield, CNPC, Panjin 124010, China

litailu19821028@163.com

Keywords: Thermodynamic, CHP, EGS, Flash, Organic Rankine cycle

ABSTRACT

As a kind of clean geothermal resource, hot dry rocks (HDR) has huge reserves in the earth's crust, and the power generation technology of HDR has simple structure and low input cost compared with the traditional power generation technology. Therefore, this study selects four combined heat and power (CHP) systems to improve the utilization of heat sources which is dry hot rock. The four systems are: combined heat and power (CHP) system based on single-stage flash (SF), double-stage flash (DF) and single-stage flash ORC (SFORC). The power generation efficiency and CHP efficiency were selected as the target parameters to optimize the parameters such as flash temperature and evaporation temperature of different CHP systems. Considering that the geothermal fluid is in the gas-liquid mixed state at the production well, so the dryness of the geothermal source has a crucial influence on the power generation and heat supply of CHP systems, and the best CHP system suitable for different dryness of geothermal fluids is screened out by comparing and analyzing the four optimized systems. The results show that the overall CHP efficiency is much higher than pure power generation efficiency. And the CHP efficiency of different systems using the back pressure of condenser for heating is 49.7%~67.5% higher than that without the back pressure, but the power generation efficiency is relatively reduced by 15.7%~16.8%. When the heat source temperature is 150℃ and the dryness is changed from 0.1 to 0.9, the power generation performance of the CHP system based on DF and SFORC is higher than that of the SF-based CHP system, while the heating performance and overall CHP performance of the SF-based CHP system is higher than that of the other three systems, and this phenomenon is more obvious when the condenser back pressure is not used.

1. INTRODUCTION

In recent years, geothermal energy has been widely concerned because of its advantages of green, stable, abundant, and renewable compared with fossil energy [1] [2] [3]. Geothermal resources are mainly composed of hydrothermal resources and hot dry rock (HDR) resources and the temperature of HDR is usually in the range of 150℃ to 650℃. Conservatively speaking, the energy stored in HDR is equivalent to 30 times the total energy of oil, natural gas and coal in the world [4]. Therefore, HDR has become the most potential geothermal power resource, but it cannot form hydrothermal geothermal resources because of its poor water permeability, and the large amount of thermal energy stored in rock mass is still difficult to directly utilize at present. Therefore, people develop and utilize HDR based on the concept of enhanced or engineered geothermal system (EGS) [5-7]. The principle is that after heat transfer between heat stored in HDR and injected water, water/steam can be extracted up to 150℃~200℃, which can be used for power generation through heat exchange and ground circulation devices, and then the discharged fluid can be re-injected into the reservoir to form a circulating loop.

Some energy conversion technologies that can be commercialized in geothermal power generation include the organic Rankine cycle (ORC) [8-9], single-stage and multi-stage flashes [10-11], direct steam expansion, organic binary Rankine cycles [12-13] and two-phase flow expander. Yari et al. [14] showed that the ORC system with IHE with R123 as the working fluid was found to have a maximum first-law efficiency of 7.65%. Feng et al. [15] found that the optimal exergy efficiency and heat exchanger area per unit net power output (APR) of regenerated ORC were 59.93% and 3.07 m^2/kW, respectively, which were 8.10% and 15.89% higher than that of basic ORC. Jalilinasrabady et al. [16] investigated the total exergy available of Sabalan production wells was calculated to be 111 MW for the single flash system, and 114 MW for the double flash system, so the double flash system is recommended. Sarr et al. [17] proposed six different modifications to the double flash plant. The research shows that the interstage heating process can increase the specific output of the equipment by about 5%, decrease the liquid content in the low-pressure turbine by about 50%, and reduce the cooling capacity required by the equipment by about 10%. Zhao et al. [18] modeled the flash binary geothermal power generation system with ORC as a subsystem in steady state, and found that the improvement of system economic performance is at the cost of system thermodynamic performance degradation. Zeyghami et al. [19] studied the performance of a combined flash-binary geothermal power cycle at a geothermal fluid temperature between 150℃ and 250℃. It was found that there is an optimum separator pressure to minimize the overall effective energy destruction of the cycle. The thermodynamic performance and technical economic analysis of the composite power cycle of EGS were carried out by Lu et al [20]. The results show that the economic performance of the DF system is the best and the technical and economic performance of FORC and DFORC is better than that of the SF system.

In order to make high-efficiency multi-level utilization of geothermal sources, in recent years, the combined heat and power system (CHP) composed of heating devices based on geothermal power generation has attracted much attention from the academic community [21-25]. Tempesti et al. [26] reached conclusion through analysis of a micro combined heat and power (CHP) plant operating on an organic Rankine cycle (ORC): the R245fa minimized the power generation costs and overall CHP costs of systems. A novel CHP configuration is proposed by Sarah et al. [27] for providing heat to a district heating (DH) system. It is found a 75/50 DH system connection has better performance than a parallel or series CHP. They also found that superheating increases the power for dry/isentropic fluids at the high ORC outlet temperature by comparing the series/parallel configuration for a low- temperature

geothermal CHP plant [28]. Farrokhi et al. [29] investigated the maximum net power output at a geothermal fluid temperature of 84.1℃ and proposed improvements in expanders and generators to improve cycle power efficiency. Jang et al. [30] concluded that if the CHP performance can be improved by increasing the volume expansion ratio and the isentropic efficiency of the expander, the post-heater must be added.

In order to make efficiency use of HDR resources, this paper aim to reuse the waste heat after power generation for heating in the EGS. Therefore, three different configurations (SF, DF, SFORC) of CHP systems are proposed based on the above researches. This study selects 150℃ geothermal fluid to select the best operating conditions of three CHP systems were optimized respectively under the variable heat source dryness. Meanwhile, compare the changes of thermodynamic parameters of systems in two cases of using and not using condenser back pressure. Finally, three different configurations of CHP systems are compared and analyzed in order to provide theoretical basis for geothermal plants in the actual project of HDR development.

2. ANALYSIS OF DIFFERENT CHP MODELS

The four pictures in Figs. 1~4 are respectively the CHP system based on different power generation cycles. The thermal power part of the cogeneration system is to install heat exchangers for ordinary residential heating by using the back pressure of condenser and the waste heat of recharge water (This article will discuss the use of condenser back pressure or no use as two cases). But there are certain differences in the circulation structure used for power generation.

The power generation part of Fig. 1 is a single-stage flash (SF) system, in which the high-temperature and high-pressure geothermal fluid is first taken out of the production well and then passed through a flash separator/separator for gas-liquid separation (whether flashing is performed according to the optimization results under different systems and working conditions). The separated high-temperature saturated liquid is heat-transferred by the heat exchanger for user heating, and the high-temperature saturated gas pushes the steam turbine to generate electricity, then it flows into the condenser and is condensed into a saturated liquid, after that mixes with the heat-transferred liquid into the injection well to complete the entire cogeneration process.

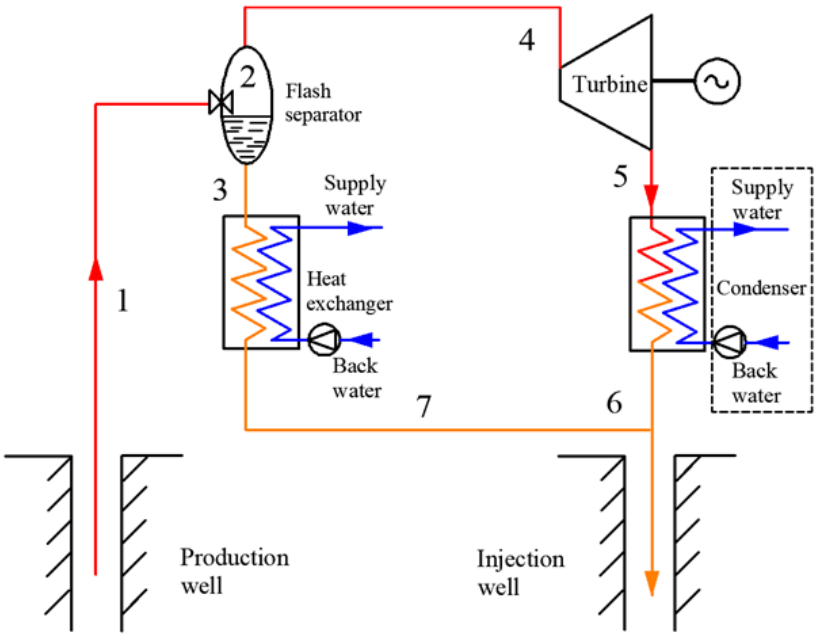

Figure 1: Schematic diagram of the SF-based CHP system.

Double-stage flash (DF) power generation system adds a secondary flash separation process on the basis of single-stage flash, as shown in Fig. 2. The saturated liquid of geothermal fluid after first-stage flash separation does not enter the heat exchanger directly, but passes through a secondary flash separator having a pressure drop, the saturated liquid is subjected to vacuum separation, and the saturated liquid after the second separation is mixed with the steam at the outlet of the high-pressure turbine and then flows through the low-pressure turbine to continue the expansion power generation. The rest of the process is exactly the same as the single-stage flash (SF) system.

The single-stage flash ORC (SFORC) system shown in Fig. 3 is based on the single-stage flash with the addition of organic Rankine cycle (ORC), which is used to absorb the heat of the saturated liquid at the outlet of the separator for power generation. The saturated liquid passes through the evaporator to vaporize the organic working fluid in the circulation to drive the steam turbine to generate electricity, and then the organic working fluid vapor enters the condenser to be condensed into a saturated liquid, which is pressurized by the working medium pump and then enters the evaporator again for heat exchange to complete a cycle. The rest of the process of the SFORC system is consistent with the SF system.

The temperature entropy diagrams of SF, DF and ORC systems are shown in Fig. 4. The choice of working fluid in the ORC unit is R245fa, and its characteristics are shown in Table 1. Meanwhile, the simulation conditions for all CHP systems are shown in Table 2.

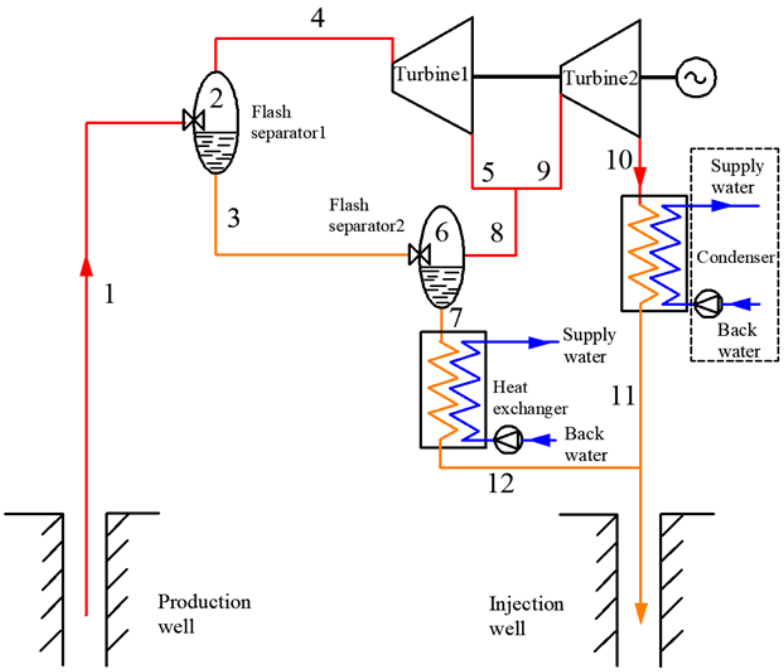

Figure 2: Schematic diagram of the DF-based CHP system.

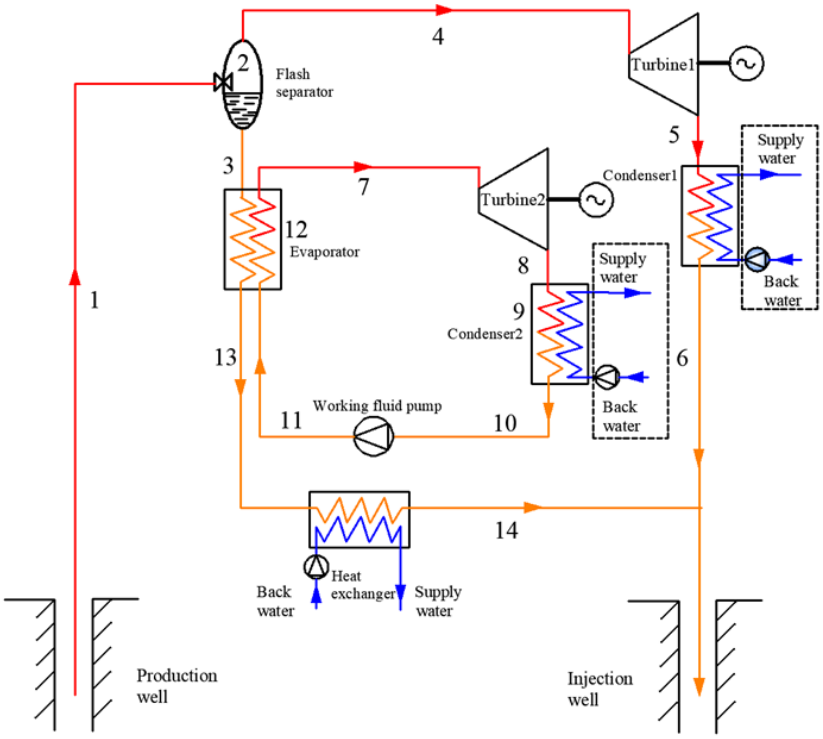

Figure 3: Schematic diagram of the SFORC-based CHP system.

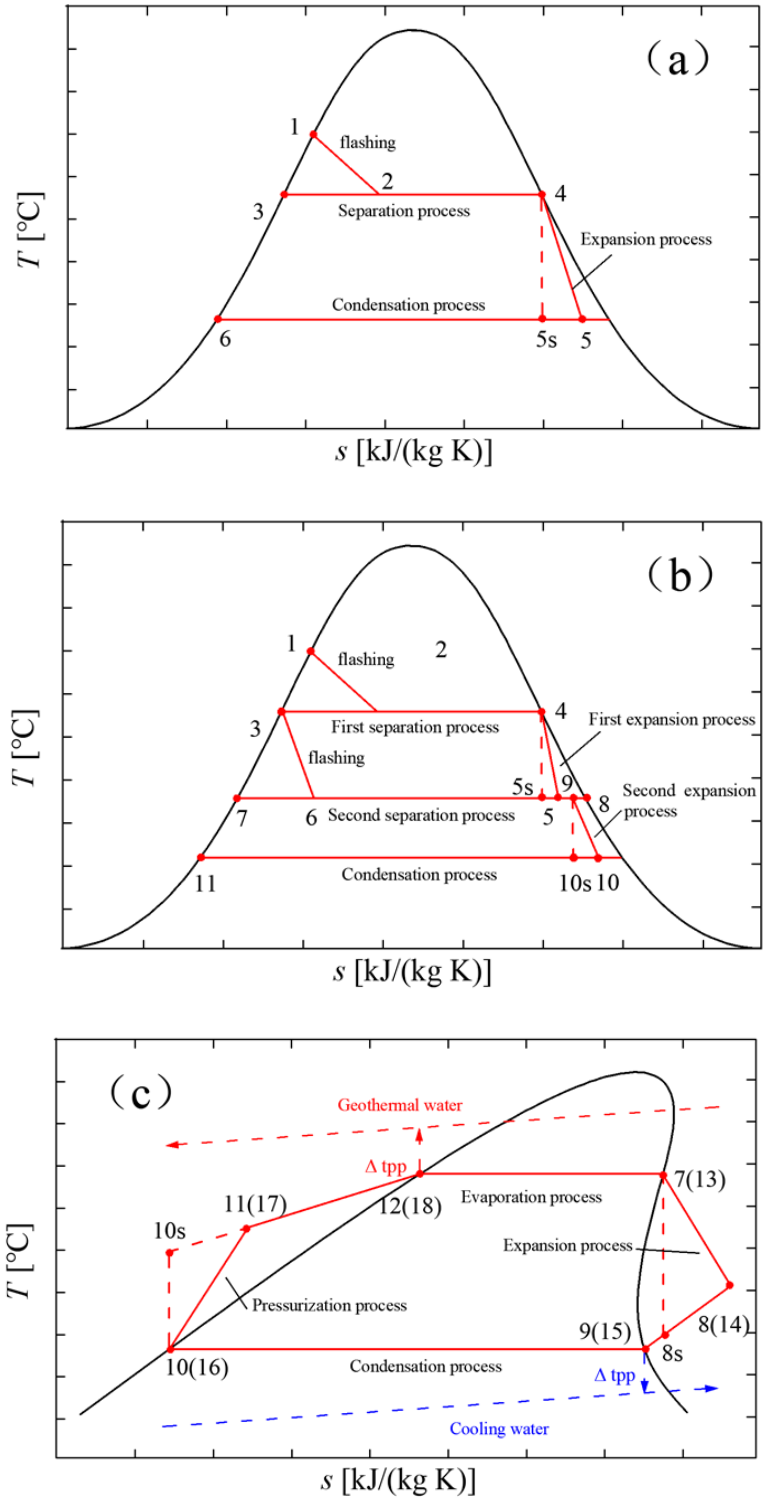

Figure 4: T-s diagrams of the SF, DF, and ORC power cycles. (a) T-s diagram of the SF; (b) T-s diagram of the DF; (c) T-s diagram of the ORC used in FORC and DFORC systems.

Table 1:Thermodynamic properties of R245fa.

Substance	Physical data				Environmental data			Source
	M(g/mol)	T_b(℃)	T_{cri}(℃)	P_{cri}(Mpa)	ALT(yr)	ODP	GWP (100yr)	
R245fa	134.05	14.90	154.05	3.640	7.6	0	1030	[31]

Table 2: Condition of simulation for the CHP systems

Items	Parameters
Ambient temperature (℃)	20
Ambient pressure (kPa)	101.3
Geothermal water temperature (℃)	150
Mass flow rate of geothermal water (kg/s)	45
Pinch point temperature difference of evaporator (℃)	5
Pinch point temperature difference of condenser (℃)	5
Condensation temperature of condenser (℃)	50
Inlet temperature of cooling water/ return water temperature (°C)	35
Outlet temperature of cooling water/ supply water temperature (°C)	45
Isentropic efficiency of flashing device (%)	75
Isentropic efficiency of turbine (%)	75
Isentropic efficiency of working fluid pump (%)	60
Isentropic efficiency of cooling water pump (%)	75
Turbine mechanical efficiency (%)	95
Generator efficiency (%)	95

3. MATHEMATICAL MODELING

According to the first law of thermodynamics and the second law, the mathematical model of each part of the system is established. To facilitate the establishment of the mathematical model and to simplify the analysis, the following assumptions are made:

(1) Systems are modeled under steady state conditions.

(2) The three systems of cold and geothermal fluid and the various components of the system operate in steady state.

(3) The pinch point temperature difference is the same at the geothermal fluid and the cold source.

(4) Changes in kinetic and potential energy of organic working fluids in the system are ignored.

(5) The pressure drop and friction loss of organic working fluids in flash devices, evaporators, condensers, heat exchangers and pipes, as well as heat losses in pipes are ignored.

(6) Energy loss during mixing of organic media in steam turbines is ignored.

(7) The pure water properties are used instead of the geothermal fluid.

Systems containing single-stage flash separator are subject to a constraint of $1(\text{bar}) < P_2 \leq P_1$ and systems with double-stage flash separators is constrained by $\begin{cases} 1(\text{bar}) < P_2 \leq P_1 \\ 0.6(\text{bar}) < P_6 \leq P_2 \end{cases}$.

3.1 Thermodynamic modeling

According to the first law of thermodynamics, the heat and mass balance of each component of the system is as follows:

$$\sum \dot{m}_{in} = \sum \dot{m}_{out} \tag{1}$$

$$\dot{Q} + \dot{W} = \sum(\dot{mh})_{out} - \sum(\dot{mh})_{in} \tag{2}$$

Where the Ẇ and Q̇ represent heat load and working capacity; m and h denote the mass flow rate and the specific enthalpy; the subscripts in and out denote the inlet and outlet of each component.

The energy interaction quality of each component was evaluated according to the second law of thermodynamics (exergy) analysis. Through the exergy analysis of the system, the irreversible damage caused by the destruction of the fire can be emphasized. The exergy balance of each part of the cycle can be expressed as:

$$\dot{I} = \dot{E}_Q + \dot{W} + \sum \dot{E}_{in} - \sum \dot{E}_{out} \tag{3}$$

$$\dot{E}_Q = \sum \dot{Q} \left(1 - \frac{T_0}{T}\right) \tag{4}$$

$$\dot{Ex} = \dot{M} \cdot ex \tag{5}$$

$$ex = (h - h_0) - T_0(s - s_0) \tag{6}$$

Where the İ is the irreversible loss of each component of the system, and the $\dot{E}_Q$ is net exergy transfer by heat transfer at temperature, Here e is the specific flow exergy, h and s are the specific enthalpy and entropy of the geothermal fluid at the specific state. The subscript 0 represents a property in a dead state. Where $\dot{M}$ represents the mass flow at each state point. Table 2 gives the mass, energy balance and exergy failure equations of each component taking DFORC-based CHP system as an example.

The net output power of the system is determined by the following formula:

$$W_{net} = \eta_m \eta_g \sum W_{ti} - \sum W_{pi} - \sum W_{cp} \tag{7}$$

Where the η_m and the η_g are the mechanical efficiency and power generation efficiency of the turbine, respectively.

The thermal power generated for heating is:

$$W_{th} = \eta_c \sum Q_{ci} + \eta_{he} Q_{he} \tag{8}$$

Where the subscript c represents the condenser and the he is the heat exchanger.

The power generation efficiency of the system is:

$$\eta_g = \frac{W_{net}}{Q_{in}} \tag{9}$$

The Q_{in} represents the heat at the entrance of the geothermal fluid.

The overall thermal efficiency of CHP system is expressed by the following formula:

$$\eta_{CHP} = \frac{W_{th} + W_{net}}{Q_{in}} \tag{10}$$

Table 3:The mass, energy and exergy equations of each component in DFORC-based CHP system.

Components	Mass balance	Energy balance	Exergy balance
Flashing device 1	$\dot{m}_1 = \dot{m}_3 + \dot{m}_4$	$\dot{m}_1 h_1 = \dot{m}_3 h_3 + \dot{m}_4 h_4$	$\dot{I}_{swp1} = \dot{m}_1 e_1 - \dot{m}_3 e_3 - \dot{m}_4 e_4$
Turbine 1	$\dot{m}_4 = \dot{m}_5$	$\dot{W}_{t1} = \dot{m}_4 h_4 - \dot{m}_5 h_5$	$\dot{I}_{t1} = \dot{m}_4 e_4 - \dot{m}_5 e_5 - \dot{W}_{t1}$
Flashing device 2	$\dot{m}_6 = \dot{m}_7 + \dot{m}_8$	$\dot{m}_6 h_6 = \dot{m}_7 h_7 + \dot{m}_8 h_8$	$\dot{I}_{swp2} = \dot{m}_6 e_6 - \dot{m}_7 e_7 - \dot{m}_8 e_8$
Turbine 2	$\dot{m}_9 = \dot{m}_{10}$ $\dot{m}_9 = \dot{m}_8 + \dot{m}_5$	$\dot{W}_{t2} = \dot{m}_9 h_9 - \dot{m}_{10} h_{10}$	$\dot{I}_{t2} = \dot{m}_9 e_9 - \dot{m}_{10} e_{10} - \dot{W}_{t2}$
Condenser 1	$\dot{m}_{10} = \dot{m}_{11}$	$\dot{Q}_{c1} = \dot{m}_{10} h_{10} - \dot{m}_{11} h_{11}$	$\dot{I}_{t2} = \dot{m}_{10} e_{10} - \dot{m}_{11} e_{11}$
ORC - evaporator	$\dot{m}_7 = \dot{m}_{12}$ $\dot{m}_{13} = \dot{m}_{17}$	$\dot{m}_7 h_7 + \dot{m}_{17} h_{17}$ $= \dot{m}_{12} h_{12} + \dot{m}_{13} h_{13}$	$\dot{I}_e = \dot{m}_7 e_7 + \dot{m}_{17} e_{17}$ $-\dot{m}_{12} e_{12} + \dot{m}_{13} e_{13}$
ORC - turbine	$\dot{m}_{13} = \dot{m}_{14}$	$\dot{W}_{t3} = \dot{m}_{13} h_{13} - \dot{m}_{14} h_{14}$	$\dot{I}_{t3} = \dot{m}_{13} e_{13} - \dot{m}_{14} e_{14} - \dot{W}_{t3}$
ORC - condenser	$\dot{m}_{14} = \dot{m}_{16}$	$\dot{Q}_{c2} = \dot{m}_{14} h_{14} - \dot{m}_{16} h_{16}$	$\dot{I}_{c2} = \dot{m}_{14} e_{14} - \dot{m}_{16} e_{16}$
ORC - pump	$\dot{m}_{16} = \dot{m}_{17}$	$\dot{W}_p = \dot{m}_{17} h_{17} - \dot{m}_{16} h_{16}$	$\dot{I}_p = \dot{m}_{16} e_{16} - \dot{m}_{17} e_{17} - \dot{W}_p$
Heat exchanger	$\dot{m}_{12} = \dot{m}_{19}$	$\dot{Q}_{he} = \dot{m}_{12} h_{12} - \dot{m}_{19} h_{19}$	$\dot{I}_{he} = \dot{m}_{12} e_{12} - \dot{m}_{19} e_{19}$

4. RESULTS AND DISCUSSION

4.1 Thermodynamic optimization process

The thermodynamic process will be first optimized for systems that using condenser back pressure for heating and systems without condenser back pressure respectively, so as to screen out the best operating conditions under these two cases. Since hot dry rocks are generally located in remote and sparsely populated areas, the use of enhanced geothermal systems (EGS) for cogeneration should take into account the number and distance of surrounding buildings, and heat is more difficult to transport than electricity. In the future, heating will also be driven by electricity, such as the heavy use of heat pumps [32]. So the development and utilization of hot dry rocks should first consider the heating problem on the premise of ensuring that the power generation efficiency reaches the optimal value. Therefore, the thermodynamic optimization process is mainly based on the optimization of power generation performance. Secondly, the optimal operating conditions of different systems will be studied with the change of geothermal fluid dryness. Finally, the power generation performance, heating performance and overall CHP performance of systems will be analyzed with the dryness.

4.1.1 SF-based CHP system

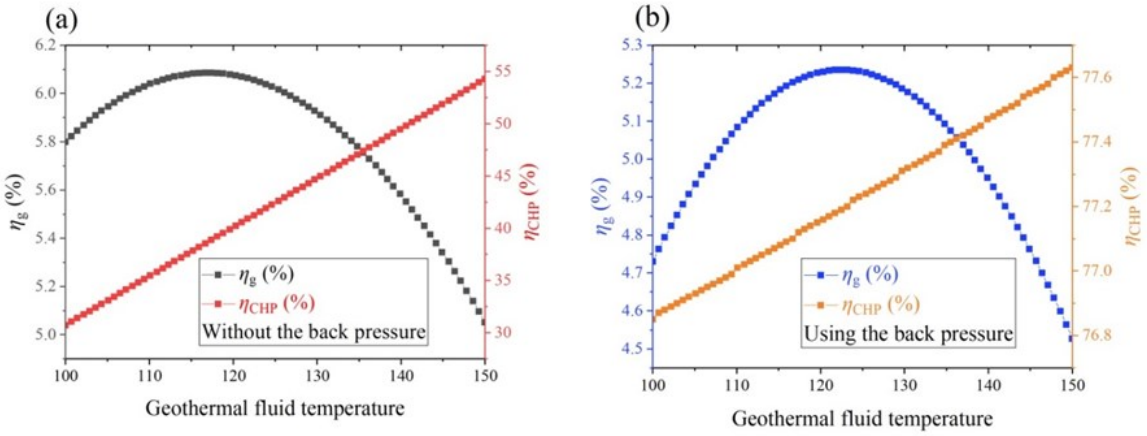

Figure5: Performance optimization process of SF-based CHP system at Tpro=150℃, x=0.1. (a) ηg without using back pressure of condenser; (b) ηCHP using back pressure of condenser.

Fig 5 shows that the variation of power generation performance and CHP performance with flash temperature in the case of heating by using back pressure of condenser and without back pressure of condenser in the SF-based CHP system at T_{pro}=150℃, x=0.1. On the one hand, it can be seen from Fig 5 (a) that the power generation efficiency η_g of SF-based CHP system first increases to a maximum value of 6.09%, at which time the flash temperature is 117℃, and then shows a decreasing trend. Because as the flash temperature rises, the mass flow rate of the steam at the outlet of the flash separator decreases while the enthalpy at the inlet of the steam turbine increases gradually. On the other hand, the higher the flash temperature, the more heat available in the system, so the variation of CHP efficiency η_{CHP} with flash temperature is gradually rising, and η_{CHP} reaches the maximum value of 54.27% at flash temperature is 150℃. As shown in the Fig 5 (b), the trend of η_g and η_{CHP} in the case of using the back pressure of condenser in SF-based CHP system is gradually the same as Fig 5 (a). The η_g reaches a maximum at a flash temperature of 123℃, which is 5.24%, and the maximum η_{CHP} is 77.2% when a flash temperature is 150℃. Therefore, it can be seen that although the η_g and η_{CHP} in SF-based CHP system has the same trend with the flash temperature in both cases, there are great differences in numerical values.

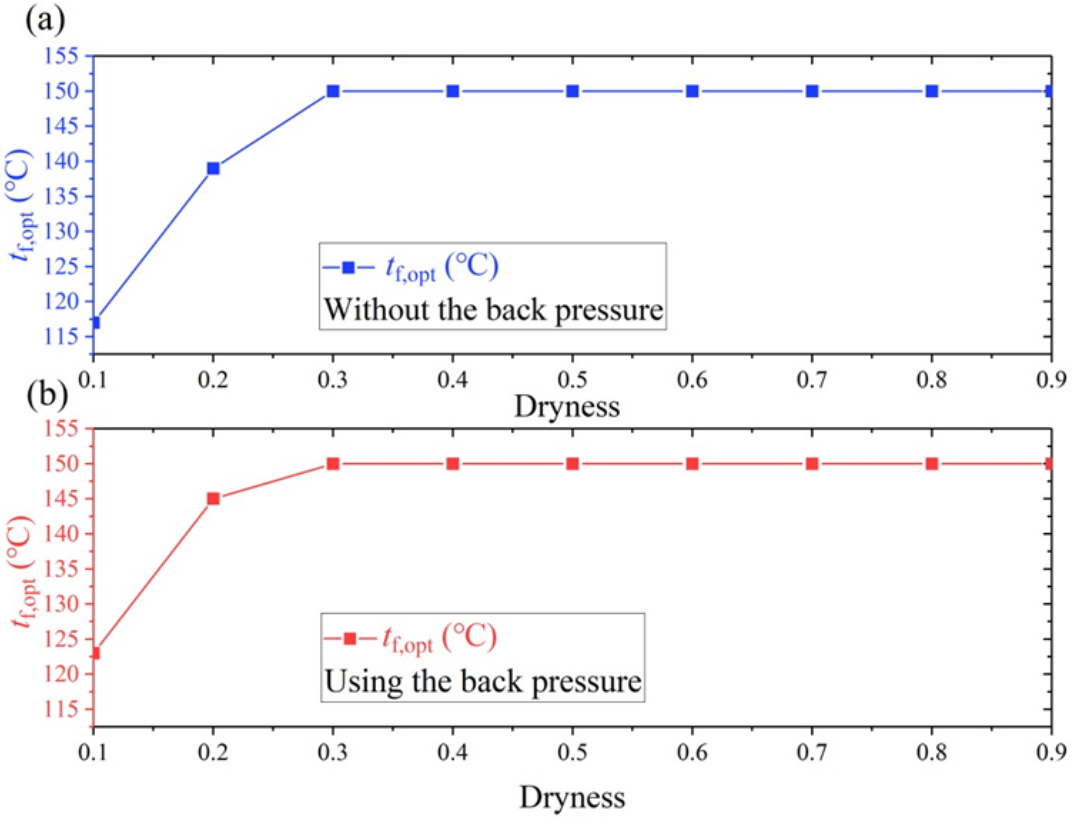

Figure6: The optimum flash temperature for different dryness in SF-based CHP system at Tpro=150℃. (a) Heating without using back pressure of condenser; (b) Heating using back pressure of condenser.

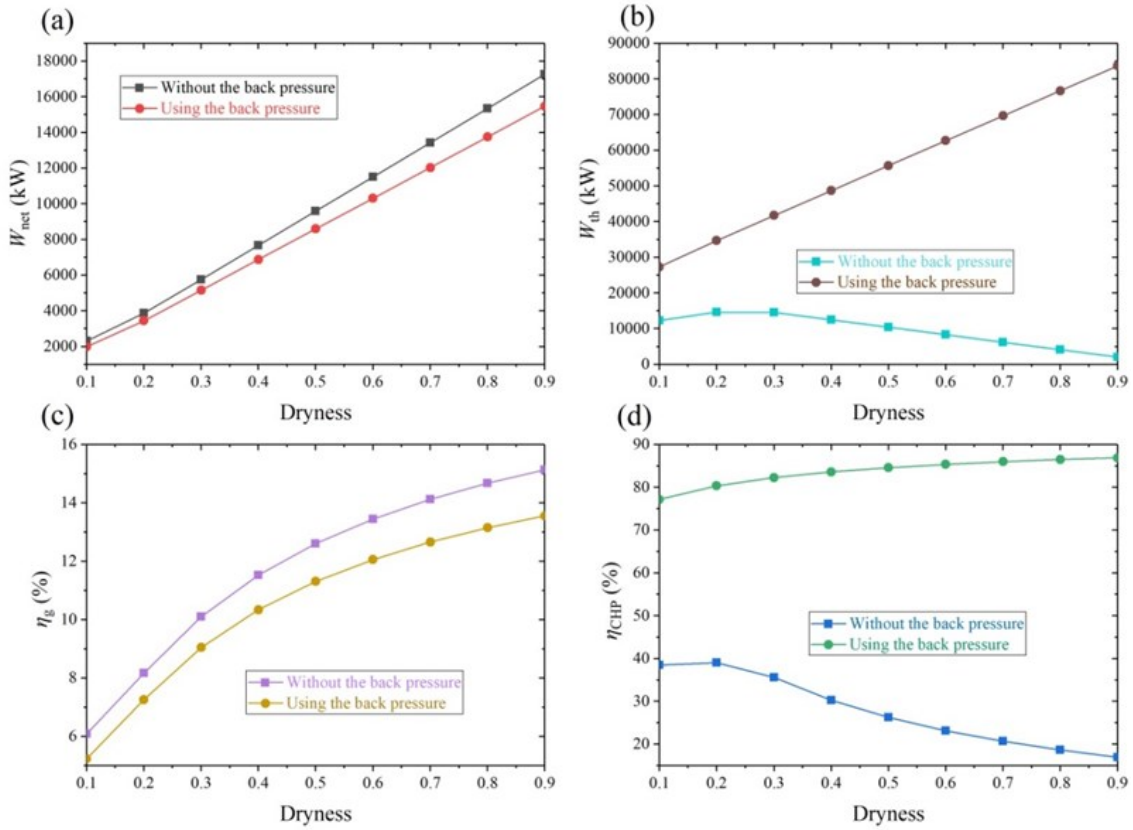

Figure7: Comparative analysis of thermodynamic parameters of SF-based CHP system in different dryness and cases; (a) the net output power Wnet; (b) the thermal power Wth; (c) the power generation efficiency ηg; (d) the CHP efficiency ηCHP.

Since the geothermal fluid after heat exchange with hot dry rock is not only liquid, it is likely to be in a gas-liquid mixed state and its dryness is not necessarily determined. Therefore, we will consider the effects of dryness changes of geothermal sources on the power generation and heating performance of different CHP systems in order to determine the optimal operating conditions of the system under various geothermal conditions. After optimizing the power generation of SF-based CHP system at different geothermal dryness, Fig 6 illustrates that the variation of optimum flash temperature with dryness in two cases. It can be seen that both the Fig 6 (a) and Fig 6 (b) have the same trend. When the dryness is less than 0.3, the optimal flash temperature of the SF-based CHP system shows an upward trend and when the dryness is greater than 0.3, the optimal flash temperature remains 150℃, which is same as geothermal fluid temperature. Therefore, at this time, the SF-based CHP system does not need to add a pressure reducing valve to perform the flashing process, and only a separator is needed to separate the gas and liquid.

Fig 7 (a) shows that the Wnet of system increases gradually with the dryness of geothermal fluid in both cases. Because the mass flow rate of the gas separated by the flash separator increases with the rise of the dryness, it can be seen that the dryness is an important factor affecting the net output power of the system. The Wnet of the system when using the back pressure of the condenser for heating is less than that when the back pressure of the condenser is not used. This is because when the back pressure of condenser is used, considering the water supply temperature required for heating is set to 45℃, the temperature of inlet and outlet water of the condenser are both increase, and the condensation temperature need to be raised to 50℃, so the Wnet of the system will be lower than if the back pressure of the condenser is not used. We can also see that the gap between two cases increase with the geothermal fluid dryness, and the Wnet difference between the two increases from 13.9% to 10.4%. For the Wth, we can see from the Fig 7 (b) that the Wth of the system which using the back pressure of condenser for heating increases with the dryness. Because the enthalpy difference between the inlet and outlet of condenser is increasing with the geothermal fluid dryness, so the Wth also increases gradually. However, without the back pressure, the Wth first increases with the dryness and then decrease, this is due to the optimal flash temperature rises with the geothermal fluid dryness, so the enthalpy difference between the inlet and outlet of heat exchanger is increasing when the dryness is less than 0.3. When the dryness is larger than 0.3, the best flash temperature remains unchanged but the mass flow rate of fluid is decreasing gradually, so the Wth also decreases. A conclusion can be drawn that the heat supplied by condenser is much larger than the heat provided by the heat exchanger. And the difference of Wth between the two cases increases from 54.9% to 97.5% with the dryness rises. The overall trend of ηg in both cases increases with dryness, as shown in Fig 7 (c). When the dryness is less than 0.3, the growth rate is faster, and when the dryness is greater than 0.3, the growth rate becomes slow. In addition, the difference of ηg between the two cases increases from 14.0% to 14.2% with the dryness. Fig 7 (d) illustrates that ηCHP of the SF-based CHP system using the back pressure of condenser increases with the geothermal fluid dryness while the ηCHP of the system without the condenser back pressure increases first and then decreases. And the difference of ηCHP between the two cases increases from 38.68% to 69.97% with the dryness.

4.1.2 DF-based CHP system

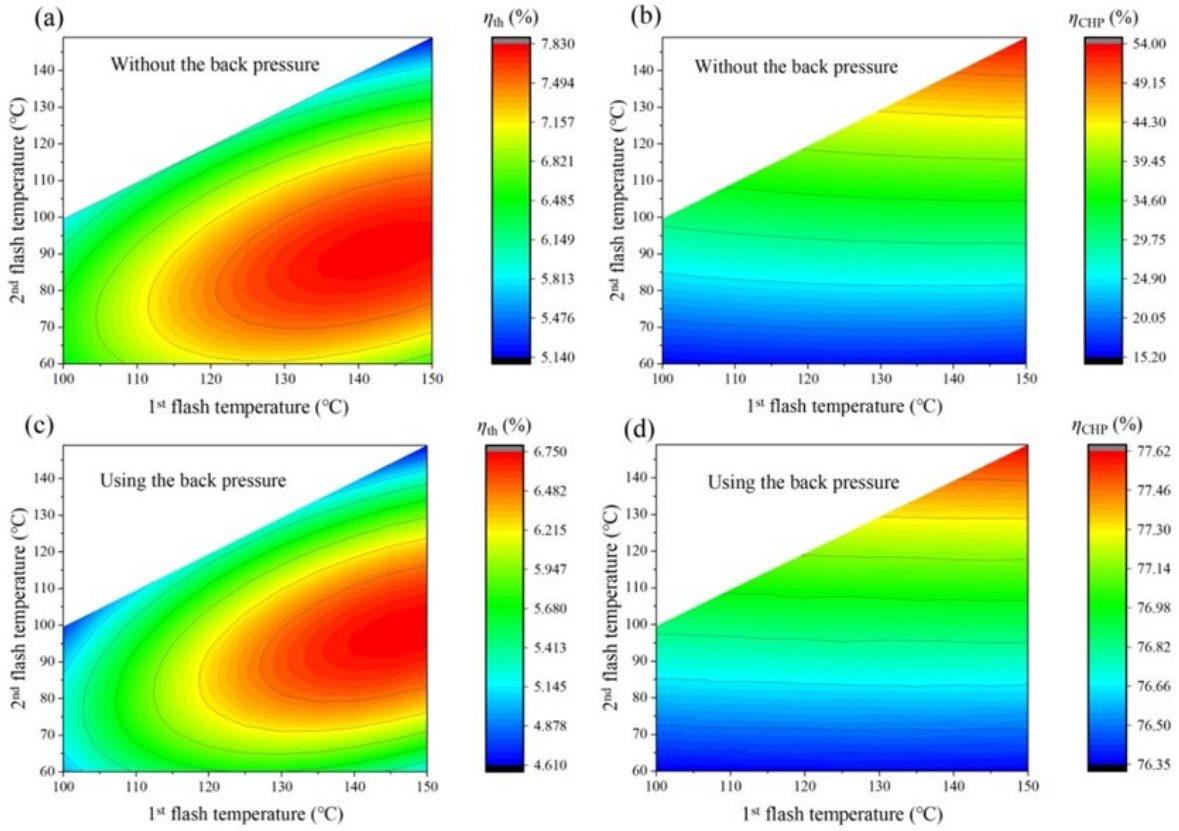

Figure8: Performance optimization process of DF-based CHP system at Tpro=150℃, x=0.1. (a) ηg without using back pressure of condenser; (b) ηCHP without using back pressure of condenser; (c) ηg using back pressure of condenser; (c) ηCHP using back pressure of condenser.

Since the DF-based CHP system has double-stage flash separator, the two-stage flash temperature will be coupled optimized. It can be seen from Fig 8 (a), (c) that η_g in both cases increases first and then decline with the 1st flash temperature and also exhibits the same trend with the 2nd flash temperature. Moreover, the η_g of system without using the condenser back pressure reaches a maximum values when the 1st flash temperature is 143℃ and the 2nd flash temperature is 91℃, and its value is 7.83%. Meanwhile when the 1st flash temperature is 147℃ and the 2nd flash temperature is 98℃, the η_g of system using the condenser back pressure reaches the maximum value of 6.75%. From the Fig 8 (b), (d), we can see that η_{CHP} of the DF-based CHP system in both cases trend to increase with 1st flash temperature and 2nd flash temperature. The η_{CHP} of system is maximized when the 1st flash temperature reaches 150℃ and the 2nd flash temperature approaches 150℃. This is because the system has the higher utilization rate of heat of geothermal fluid when the pressure reducing valve is not added to lower the flash temperature of the system, so the η_{CHP} is also better. Meanwhile, the optimal η_{CHP} of the system without back pressure is about 54.00%, while that of the system with back pressure is 77.62%.

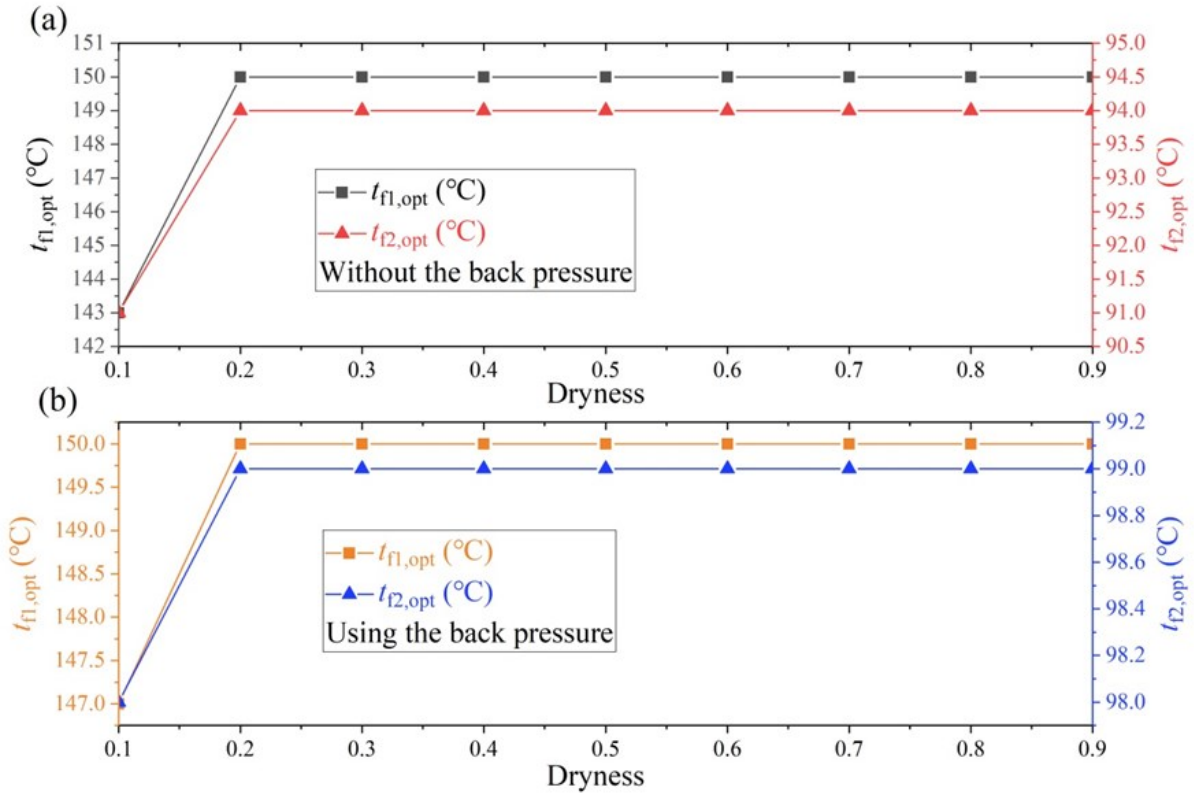

Figure 9: The optimum flash temperature for different dryness in DF-based CHP system at Tpro=150℃. (a) Heating without using back pressure of condenser; (b) Heating using back pressure of condenser.

Fig 9 shows that the selection of the best power generation conditions for the DF-based CHP system with different dryness of heat source in two cases. It can be seen that a pressure reducing valve need to be added in the 1st flash separator to reduce the 1st flash temperature when the dryness is 0.1, when the dryness increases from 0.2 to 0.9, the 1st flash temperature remains stable and the value reaches 150℃ in both cases. At the same time, the 2nd flash undergoes a change corresponding to the 1st flash temperature. At the dryness is between 0.2 and 0.9, the optimum 2nd flash temperature reaches 94°C in the system without using the back pressure and reaches 99°C in the system using back pressure. The results show that the best1st flash temperature and 2nd flash temperature of the DF-based CHP system using the back pressure are both higher than those of the system without using the back pressure.

As shown in the Fig 10 (a), we can see that the Wnet increases gradually with the geothermal fluid dryness in both cases. Meanwhile the difference between two cases increases from 409kW to 1871kW with the dryness rises. Fig 10 (c) illustrates that the ηg also increases with the dryness and the difference between two cases rises from 1.08% to 1.64%. Comparing the two parameters related to power generation performance can be seen that the system without using the back pressure of condenser has better power generation performance than the system using the back pressure. However, for the Wth and ηCHP of DF-based CHP system, it can be seen from the Fig 10 (b), (d) that the two parameters of system using the back pressure increase with the dryness and the two parameters trend to decrease with the dryness in the system without using the back pressure. Meanwhile, the difference of Wth in two cases increases from 18627kW to 82351.4kW with dryness and the difference of ηCHP increases from 47.98% to 70.55%.

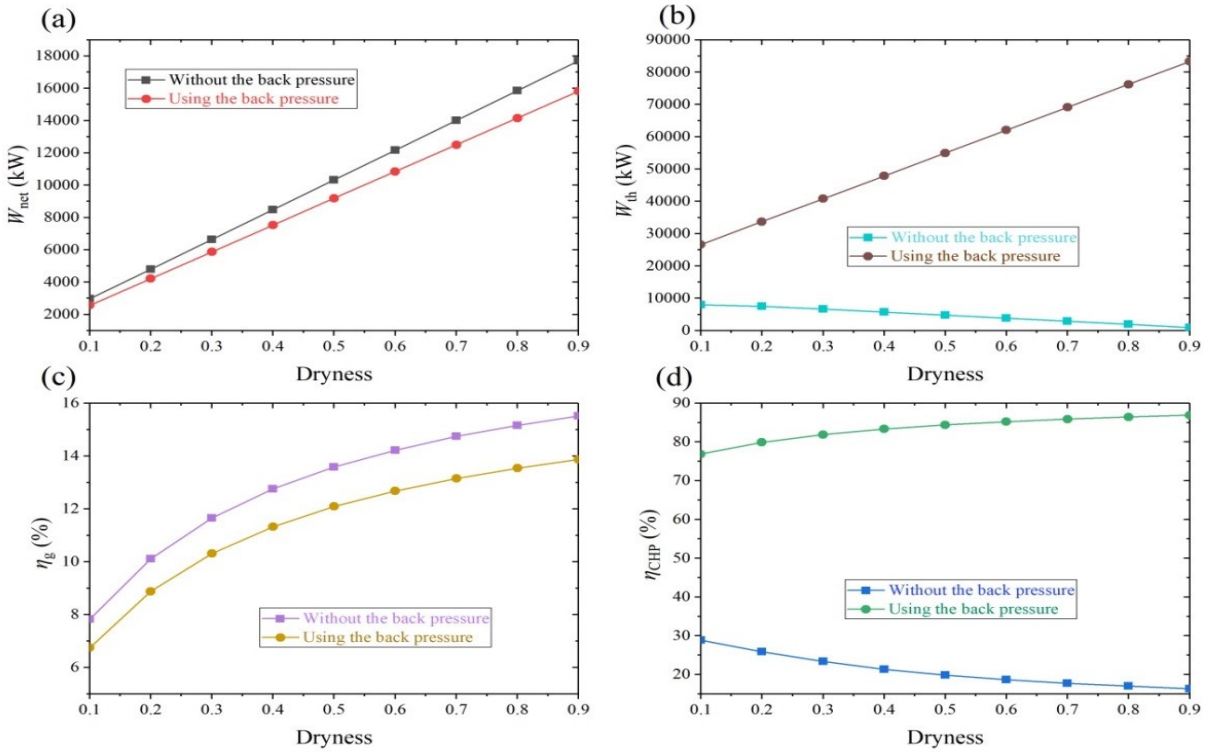

Figure10: Comparative analysis of thermodynamic parameters of DF-based CHP system in different dryness and cases; (a) the net output power Wnet; (b) the thermal power Wth; (c) the power generation efficiency ηg; (d) the CHP efficiency ηCHP.

4.1.3 SFORC-based CHP system

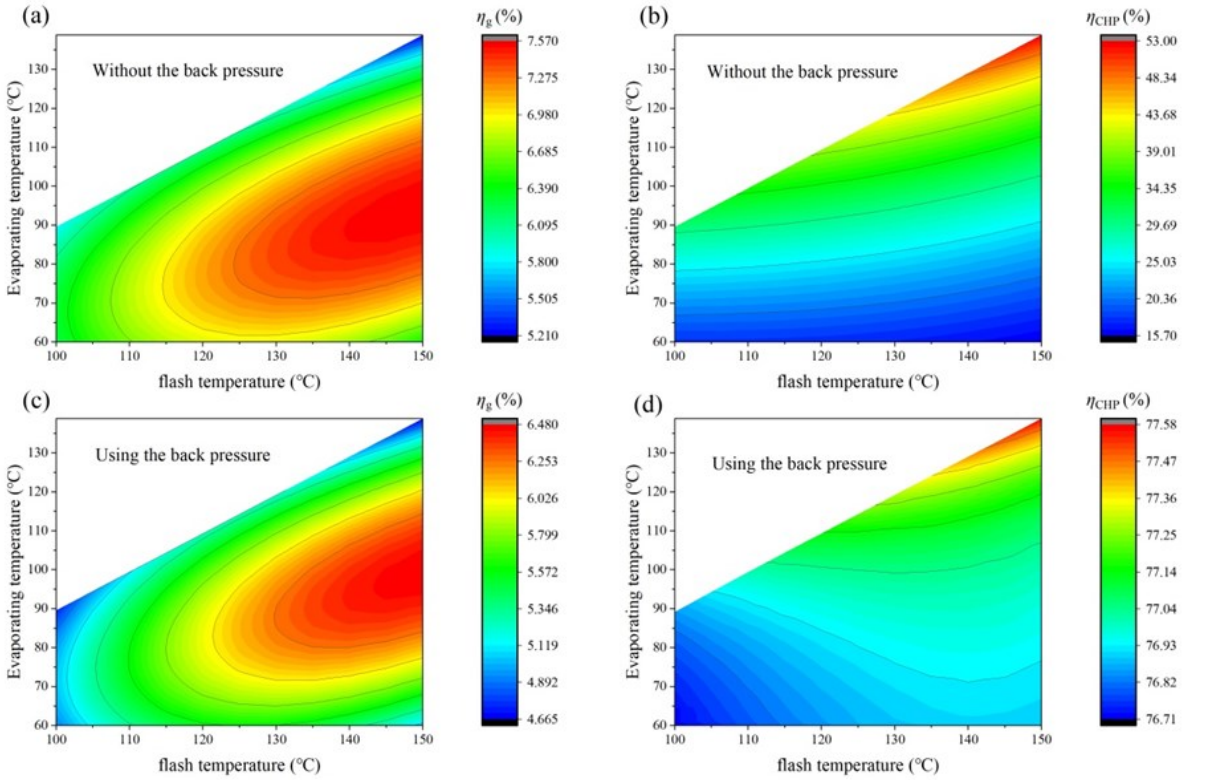

Figure11: Performance optimization process of SFORC-based CHP system at Tpro=150℃, x=0.1. (a) ηg without using back pressure of condenser; (b) ηCHP without using back pressure of condenser; (c) ηg using back pressure of condenser; (c) ηCHP using back pressure of condenser.

The optimization results of the flash temperature and evaporation temperature of SFORC system are shown in Fig 11. On the one hand, the η_g of system without using the back pressure of condenser increases with the flash temperature, and first increases and then decreases with evaporation temperature. So when the flash temperature is 150℃ and the evaporation temperature is 95℃ the η_g reaches the optimal value of 7.57%. Meanwhile, the η_g of system using the back pressure has the same tendency, and achieves a best value of 6.48% at a flash temperature of 150℃ and an evaporation temperature of 99℃. On the other hand, in both cases, the η_{CHP} of system increases with flash temperature and evaporation temperature. The η_{CHP} of a system without using back pressure achieves an optimal value of 53.00% while it reaches 77.58% in a system using back pressure.

The simulation results show that the optimal flash temperature and evaporation temperature of SFORC-based CHP system do not change with the dryness of geothermal fluid in both cases. Therefore, the diagram of the optimum operating condition varying with dryness is omitted here.

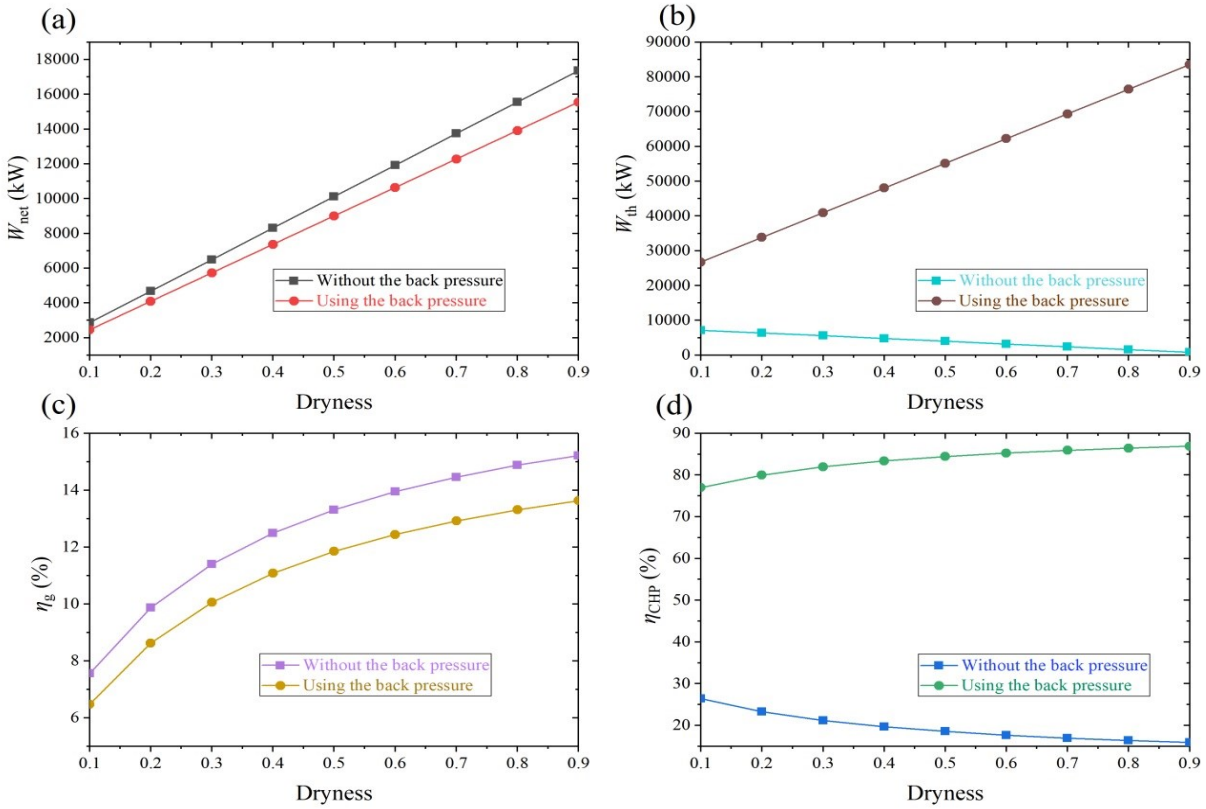

Figure12: Comparative analysis of thermodynamic parameters of SFORC-based CHP system in different dryness and cases; (a) the net output power Wnet; (b) the thermal power Wth; (c) the power generation efficiency ηg; (d) the CHP efficiency ηCHP.

Fig 12 (a) shows that W_{net} of the SFORC-based CHP system increases gradually with the geothermal fluid dryness in both cases. Meanwhile the difference between two cases increases from 413kW to 1814kW with the dryness rises. Fig 12 (c) illustrates that the η_g also increases with the dryness and the difference between two cases rises from 1.09% to 1.59%. Comparing the two parameters related to power generation performance can be seen that the system without using the back pressure of condenser has better power generation performance than the system using the back pressure. However, for the W_{th} and η_{CHP} of SFORC-based CHP system, it can be seen from the Fig 12 (b), (d) that the two parameters of system using the back pressure increase with the dryness and trend to decrease in the system without using the back pressure. Meanwhile, the difference of W_{th} in two cases increases from 19607kW to 82776.7kW with dryness and the difference of η_{CHP} increases from 50.55% to 70.98%.

Firstly, analysis of the part can be concluded that the flash temperature needs to be adjusted by flash separator when the dryness is 0.1, while the flash separator in SF-based CHP system and the 1st flash separator in DF-based CHP system only need to play a separation role when the dryness is larger than 0.1. However, the optimal operating conditions of SFORC-based CHP system do not change with the dryness. Secondly, comparing the two cases in different systems, it can be found that the power generation performance of the system without using back pressure is better than the other, and the effect is more obvious with the dryness increases, but its heating performance and overall CHP performance are far lower than the system using the back pressure and the gap increases gradually with the dryness.

4.2 Comparison results between different systems

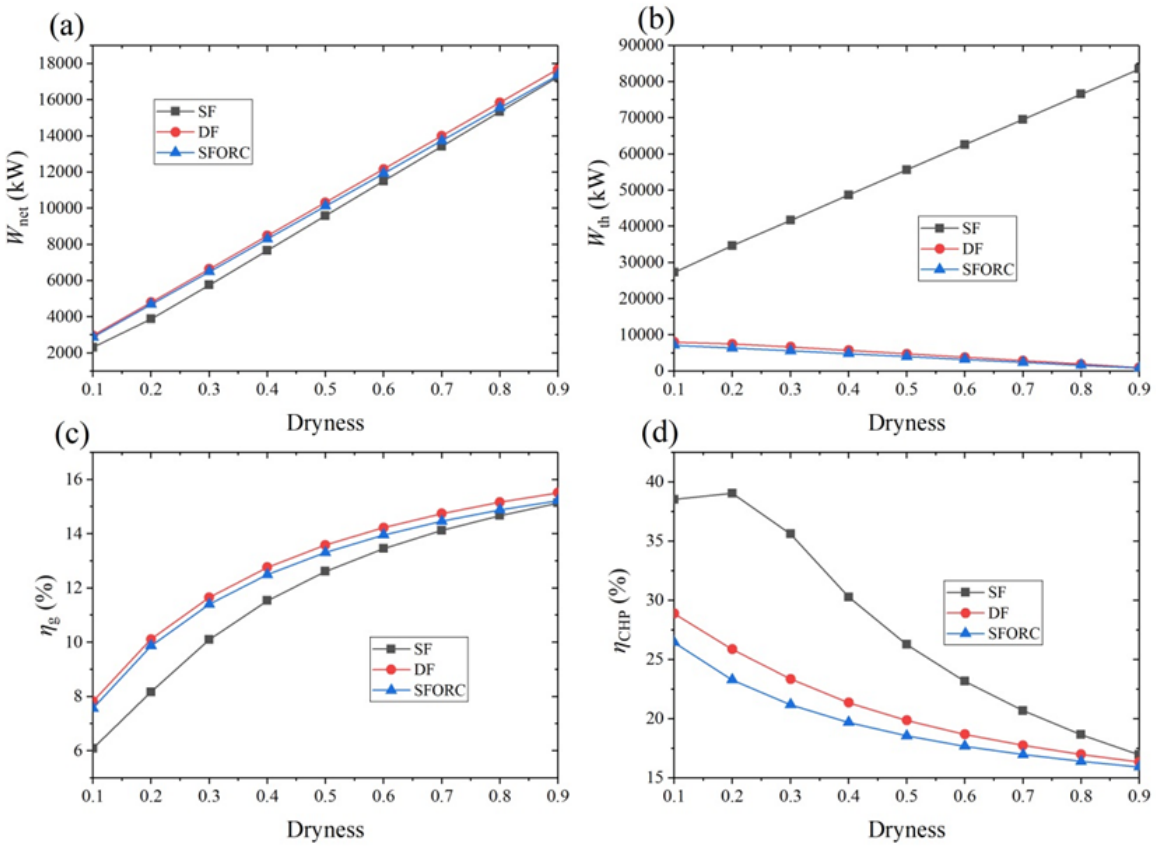

Figure13: Comparative analysis of thermodynamic parameters of different systems without using back pressure; (a) the net output power Wnet; (b) the thermal power Wth; (c) the power generation efficiency ηg; (d) the CHP efficiency ηCHP.

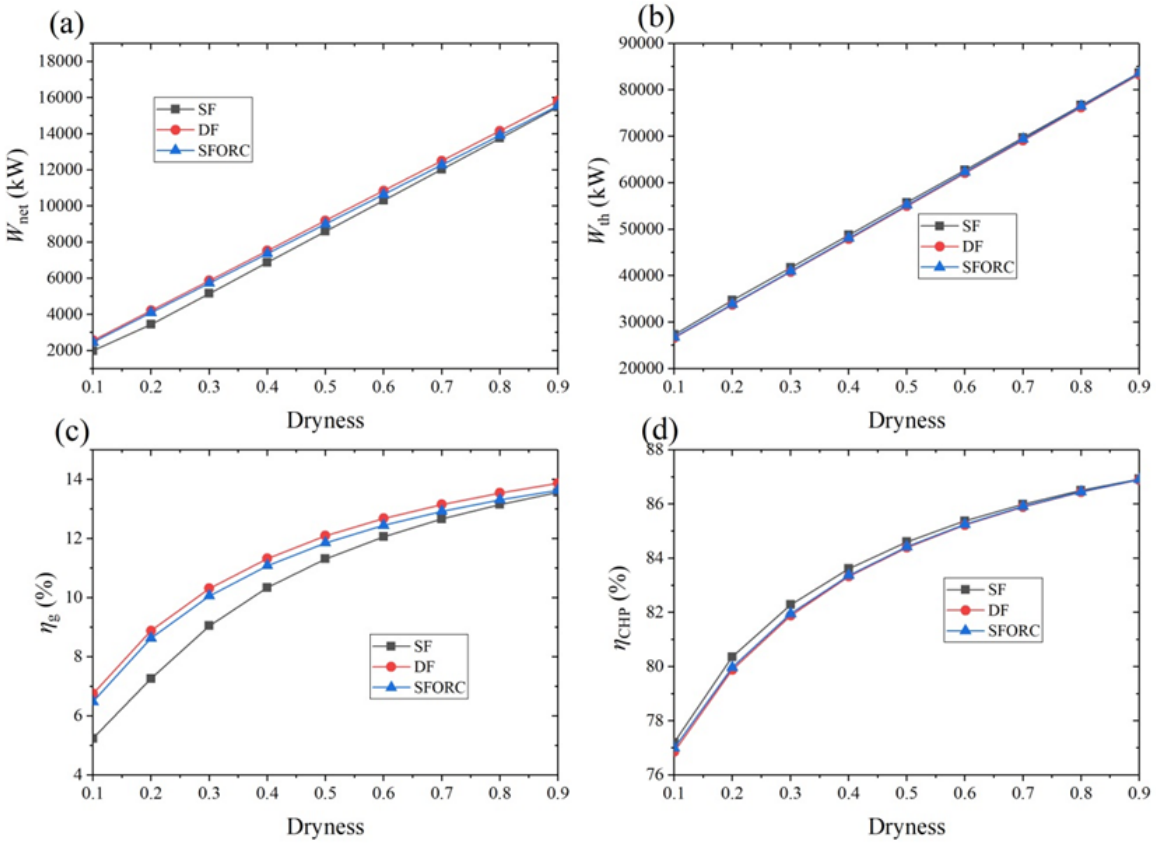

Figure14: Comparative analysis of thermodynamic parameters of different systems using back pressure; (a) the net output power Wnet; (b) the thermal power Wth; (c) the power generation efficiency ηg; (d) the CHP efficiency ηCHP.

In this section, the power generation performance, heating performance and overall CHP performance of different systems will be compared to select the recommended CHP system. From the Fig 13 we can see the thermodynamic parameters of different CHP systems which without using the back pressure change with the dryness. Fig 13 (a), (c) show the W_{net} and η_g of DF-based CHP system is the highest among all systems under any geothermal fluid dryness, while that of SF-based CHP system is lowest. However, with the increase of dryness, the gap of power generation performance between SF-based CHP system and other systems gradually decreases. For the heat performance of systems, it can be seen from the Fig 13 (b) that the W_{th} of SF-based CHP system is much larger than that of other systems, while the difference increases gradually with the dryness. Meanwhile, the W_{th} of SFORC-based CHP system is lowest. The Fig 13 (d) illustrates the overall η_{CHP} of SF-based CHP system is the largest and that of SFORC-based CHP system is lowest in all systems, while the η_{CHP} difference between SF-based CHP system and others is declining with the dryness of geothermal fluid.

A comparison of the thermodynamic parameters between different CHP systems that using the back pressure of condenser for heating is shown in Fig 14. From the Fig 14 (a) we can see the W_{net} and η_g of each system have the same tendency as the previous case which the DF-based CHP system is the highest among all systems, and the SF-based CHP system is lowest. Meanwhile, the gap of power generation performance between SF-based CHP system and other systems gradually decreases with the increase of dryness. For the heat performance of systems, it can be seen from the Fig 14 (b) that the W_{th} of SF-based CHP system is largest but the gap between three systems is very small, and the W_{th} of these systems tends to be uniform with the dryness rises. The Fig 14 (d) illustrates the overall η_{CHP} of SF-based CHP system is the largest but the gap between three systems is also small, while the η_{CHP} of different systems tends to be the same with the dryness increases.

5. CONCLUSIONS

Through comprehensive thermodynamic optimization of different cogeneration systems (SF-based CHP system, DF-based CHP system, SFORC-based CHP system) in two cases, the optimum operating conditions of each system corresponding to different dryness of geothermal fluid are obtained. The comparative analysis of the power generation, heating and CHP performance of the three systems provides an important basis for the selection of systems and working conditions of the CHP plant. The specific conclusions drawn from the study are as follows:

(1) CHP systems have much higher heat utilization rate of geothermal fluid than pure power generation systems.

(2) The optimal flash temperature of the SF-based CHP system and DF-based CHP system varies with the geothermal fluid dryness, so attention should be paid to the selection of optimum operating conditions.

(3) The steam content the outlet of production wells has a great influence on the operating performance of systems and the power generation performance gradually increases with the dryness.

(4) Comparing the two cases, it can be concluded that although the addition of condenser back pressure can improve the CHP efficiency of systems, it is at the expense of reducing the generation efficiency.

(5) Different systems have their own advantages and disadvantages in power generation performance and CHP performance. The SF-based system without using the back pressure of condenser is suggested because its CHP efficiency is much higher than other systems. Meanwhile, the DF-based system in all systems using the back pressure is recommended due to its high power generation efficiency.

(6) HDR plants should select the configuration of systems according to the surrounding heat demand, and select the system operating conditions according to heat source dryness at the outlet of the production well.

REFERENCES

[1] Lin L, Zhen X H, Zhan M P.: The utilization and development prospect of geothermal energy resource, Resources and Industries, 8, (2006), 20-23.

[2] Hofmann H, Babadagli T, Zimmermann G.: Hot water generation for oil sands processing from enhanced geothermal systems: process simulation for different hydraulic fracturing scenarios, Applied energy, 113, (2014), 524-547.

[3] Quattrocchi F, Boschi E, Spena A, et al.: Synergic and conflicting issues in planning underground use to produce energy in densely populated countries, as Italy: geological storage of CO2, natural gas, geothermics and nuclear waste disposal, Applied energy, 101, (2013), 393-412.

[4] Brown D.: The US hot dry rock program-20 years of experience in reservoir testing//Proc, World Geothermal Congress, (1995), 2607-2611.

[5] Brown D W, Duchane D V.: Scientific progress on the Fenton Hill HDR project since 1983, Geothermics, 28, (1999), 591-601.

[6] Genter A, Evans K, Cuenot N, et al.: Contribution of the exploration of deep crystalline fractured reservoir of Soultz to the knowledge of enhanced geothermal systems (EGS), Comptes Rendus Geoscience, 342, (2010), 502-516.

[7] Tenma N, Yamaguchi T, Zyvoloski G.: The Hijiori hot dry rock test site, Japan: evaluation and optimization of heat extraction from a two-layered reservoir, Geothermics, 37, (2018), 19-52.

[8] Xu T, Yuan Y, Jia X, et al.: Prospects of power generation from an enhanced geothermal system by water circulation through two horizontal wells: A case study in the Gonghe Basin, Qinghai Province, China, Energy, 148, (2018), 196-207.

[9] Zhang F Z, Xu R N, Jiang P X.: Thermodynamic analysis of enhanced geothermal systems using impure CO2 as the geofluid, Applied Thermal Engineering, 99, (2016), 1277-1285.

[10] Bina S M, Jalilinasrabady S, Fujii H.: Exergoeconomic analysis and optimization of single and double flash cycles for Sabalan geothermal power plant, Geothermics, 72, (2018), 74-82.

[11] Clarke J, McLeskey Jr J T.: The constrained design space of double-flash geothermal power plants, Geothermics, 51, (2014), 31-37.

[12] Wang J, Wang J, Dai Y, et al.: Thermodynamic analysis and optimization of a flash-binary geothermal power generation system, Geothermics, 55, (2015), 69-77.

[13] DiPippo R.: Second law assessment of binary plants generating power from low-temperature geothermal fluids, Geothermics, 33, (2004), 565-586.

[14] Yari M.: Exergetic analysis of various types of geothermal power plants, Renewable energy, 35, (2010), 112-121.

[15] Feng Y, Zhang Y, Li B, et al.: Sensitivity analysis and thermoeconomic comparison of ORCs (organic Rankine cycles) for low temperature waste heat recovery, Energy, 82, (2015), 664-677.

[16] Jalilinasrabady S, Itoi R, Valdimarsson P, et al.: Flash cycle optimization of Sabalan geothermal power plant employing exergy concept, Geothermics, 43, (2012), 75-82.

[17] Sarr J A R, Mathieu-Potvin F.: Improvement of Double-Flash geothermal power plant design: A comparison of six interstage heating processes, Geothermics, 54, (2015), 82-95.

[18] Zhao Y, Wang J.: Exergoeconomic analysis and optimization of a flash-binary geothermal power system, Applied energy, 179, (2016), 159-170.

[19] Zeyghami M.: Performance analysis and binary working fluid selection of combined flash-binary geothermal cycle, Energy, 88, (2015), 765-774.

[20] Lu X, Zhao Y, Zhu J, et al.: Optimization and applicability of compound power cycles for enhanced geothermal systems, Applied energy, 229, (2018), 128-141.

[21] Qiu G, Liu H, Riffat S.: Expanders for micro-CHP systems with organic Rankine cycle, Applied Thermal Engineering, 31, (2011), 3301-3307.

[22] Qiu G, Shao Y, Li J, Liu H, Riffat SB.: Experimental investigation of a biomass-fired ORC-based micro-CHP for domestic applications, Fuel, 96, (2012), 374-382.

[23] Tempesti D, Manfrida G, Fiaschi D.: Thermodynamic analysis of two micro CHP systems operating with geothermal and solar energy, Applied Energy, 97, (2012), 609-617.

[24] Farrokhi M, Noie SH, Akbarzadeh AA.: Preliminary experimental investigation of a natural gas-fired ORC-based micro-CHP system for residential buildings, Applied Thermal Engineering, 69, (2014), 221-229.

[25] Ruzzenenti F, Bravi M, Tempesti D, et al, Salvatici E, Manfrida G, Basosi R.: Evaluation of the environmental sustainability of a micro CHP system fueled by low-temperature geothermal and solar energy, Energy Conversion and Management, 78, (2014), 611-616.

[26] Tempesti D, Fiaschi D.: Thermo-economic assessment of a micro CHP system fuelled by geothermal and solar energy, Energy, 58, (2013), 45-51.

[27] Van Erdeweghe S, Van Bael J, Laenen B, et al.: “Preheat-parallel” configuration for low-temperature geothermally-fed CHP plants, Energy Conversion and Management, 142, (2017), 117-126.

[28] Van Erdeweghe S, Van Bael J, Laenen B, et al.: Comparison of series/parallel configuration for a low-T geothermal CHP plant, coupled to thermal networks, Renewable energy, 111, (2017), 494-505.

[29] Farrokhi M, Noie SH, Akbarzadeh AA.: Preliminary experimental investigation of a natural gas-fired ORC-based micro-CHP system for residential buildings, Applied Thermal Engineering, 69, (2014), 221-229.

[30] Jang Y, Lee J.: Influence of superheat and expansion ratio on performance of organic Rankine cycle-based combined heat and power (CHP) system, Energy conversion and management, 171, (2018), 82-97.

[31] Calm J M, Hourahan G C.: Refrigerant data update, Hpac Engineering, 79, (2007), 50-64.

[32] Nami H, Arabkoohsar A.: Improving the power share of waste-driven CHP plants via parallelization with a small-scale Rankine cycle, a thermodynamic analysis, Energy, 171, (2019), 27-36.

ACKNOWLEDGMENTS

The authors gratefully acknowledge the support provided by the National Key Research and Development Program of China (Grant No. 2018YFB1501805) and the Opening Funds of State Key Laboratory of Building Safety and Built Environment And National Engineering Research Center of Building Technology (Grant No. BSBE2018-06).